A Disk Instability Model for the Quasi-periodic Eruptions of GSN 069

Xin Pan[1,2] , Shuang-Liang Li[1,2] , Xinwu Cao[3,4] , Giovanni Miniutti[5] , and Minfeng Gu[1]
[1] Key Laboratory for Research in Galaxies and Cosmology, Shanghai Astronomical Observatory, Chinese Academy of Sciences, 80 Nandan Road, Shanghai 200030,
People's Republic of China; panxin@shao.ac.cn, lisl@shao.ac.cn
[2] University of Chinese Academy of Sciences, 19A Yuquan Road, 100049, Beijing, People's Republic of China
[3] Zhejiang Institute of Modern Physics, Department of Physics, Zhejiang University, 38 Zheda Road, Hangzhou 310027, People's Republic of China
xwcao@zju.edu.cn
[4] Shanghai Astronomical Observatory, Chinese Academy of Sciences, 80 Nandan Road, Shanghai, 200030, People's Republic of China
[5] Centro de Astrobiología (CSIC-INTA), Camino Bajo del Castillo s/n, Villanueva de la Cañada, E-28692 Madrid, Spain
Received 2022 January 14; revised 2022 March 12; accepted 2022 March 22; published 2022 April 4

Abstract

GSN 069 is a recently discovered quasi-periodic eruption (QPE) source recurring about every 9 hr. The mechanism for the QPEs of GSN 069 is still unclear. In this work, a disk instability model is constructed to explain GSN 069 based on Pan et al. (PLC21), where the authors proposed a toy model for the repeating changing-look active galactic nuclei. We improve the work of PLC21 by including a nonzero viscous torque condition on the inner boundary of the disk and adopting a general form for the viscous stress torque in the Kerr metric. It is found that the 0.4–2 keV light curves, the light curves at different energy bands, and the phase-resolved X-ray spectrum of GSN 069 can all be qualitatively reproduced by our model. Furthermore, the profiles of light curves in QPEs can be significantly changed by the parameter μ in the viscous torque equation, which implies that our model may also be applied to other QPEs.

Unified Astronomy Thesaurus concepts: Magnetic fields (994); Galaxy accretion disks (562); Active galactic nuclei (16)

1. Introduction

Quasi-periodic eruptions (QPEs) are new phenomena exhibiting quasi-periodic rapid and high-amplitude bursts in soft X-ray that were reported by Miniutti et al. (2019) first in the low-mass Seyfert 2 galaxy GSN 069. The burst duration and period of GSN 069 are about 1 and 9 hr, respectively. In addition to GSN 069, four other QPE sources, i.e., RX J1301.9+2747 (Sun et al. 2013; Giustini et al. 2020), 2MASS 02314715-1020112, 2MASX J02344872-4419325 (Arcodia et al. 2021), and XMMSL1 J024916.6-041244 (Chakraborty et al. 2021), have been discovered recently. Compared with others, more physical properties of GSN 069 have been inferred, such as the central black hole mass ($M_{BH} \sim 4 \times 10^5 M_\odot$ with a factor of a few uncertainty), the X-ray spectrum in various stages during outbursts, and the nearly constant eruption period with alternating long/short QPE time separation as well as alternating strong/weak QPEs. All of these are very important for us to study the physical origin of QPEs.

Several models have been proposed to explain the physics of QPEs: radiation pressure instabilities in the transition zone between the inner advection-dominated accretion flow (ADAF) and the outer thin disk (Sniegowska et al. 2020; Pan et al. 2021, hereinafter PLC21); Roche lobe overflow from one/two stars orbiting the central black hole (Zhao et al. 2021; Metzger et al. 2022); mass overflow at pericenter from a white dwarf around a super-massive black hole (a near miss tidal disruption; King 2020); warped disk tearing (Raj & Nixon 2021); self-lensing of a binary massive black hole (Ingram et al. 2021); and star–disk collisions (Suková et al. 2021; Xian et al. 2021). These models can partly explain the outbursts of QPEs, but mainly focus on their short timescales and regular periods. So

far, there is no model that can fit both the outburst period and the X-ray spectrum of GSN 069 simultaneously. The observed X-ray spectra at various burst stages in GSN 069 have been successfully reproduced by using a constant disk blackbody plus a variable blackbody component (Miniutti et al. 2019). Together with the quasi-periodic outbursts, we notice that all these characteristics may be explained by the model of Sniegowska et al. (2020) and PLC21.

The radiation pressure dominated inner region of a standard thin disk is both thermally and viscously unstable (Shakura & Sunyaev 1973, 1976). Adopting some special values, this unstable region can be shrunken to a narrow zone between inner ADAF and outer thin disk (Sniegowska et al. 2020). This model has been successfully applied to the repeating changing-look (CL) active galactic nuclei (AGN). Due to the important role of magnetic field playing on the formation of jet/winds, PLC21 investigated how the large-scale magnetic field affects the outbursts of the unstable region and found that both the period and amplitude of outbursts can be significantly changed. However, the mass accretion rate of GSN 069 should be very high due to its high luminosity ($\sim 10^{42} \mathrm{erg\,s^{-1}}$) and a relatively small black hole mass ($\sim 4 \times 10^5 M_\odot$; Miniutti et al. 2019). In this case, the inner ADAF will disappear and the thin disk can extend to the innermost stable circular orbit (ISCO; Narayan et al. 1998). The high mass accretion rate will also result in a larger unstable inner region in a thin disk and a much longer outburst period, which is inconsistent with the behavior of QPEs. However, as shown in PLC21, this point can be resolved if we consider the effects of large-scale magnetic field, which can take away both the energy and angular momentum from the disk and decrease its temperature significantly (Cao & Spruit 2013; Li & Begelman 2014; Li & Cao 2019). In this work, we construct a disk instability model base on PLC21 to explain the quasi-periodic eruptions of GSN 069.
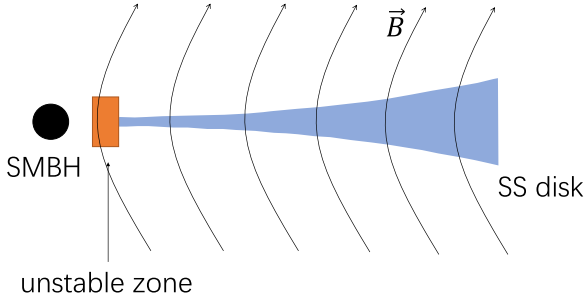
Figure 1. The schematic picture of our model. The outer blue region represents a stable thin disk dominated by gas pressure and the inner orange region is the unstable zone dominated by radiation pressure.

2. Model

2.1. Steady Outer Disk

The inner ADAF will disappear when the mass accretion rate is high enough. Therefore, the disk contains only two regions: the inner unstable and outer stable regions (see Figure 1). On the presence of a large-scale magnetic field, the unstable region can be constrained to a narrow zone just outside the ISCO. In order to improve the precision of our model, we adopt the general relativistic correction factors defined by Novikov & Thorne (1973) to modify our equations:

$$\mathscr{A} = 1 + \frac{a_*^2}{4\hat{r}^2} + \frac{a_*^2}{4\hat{r}^3}, \tag{1}$$

$$\mathscr{B} = 1 + a_*\sqrt{\frac{1}{8\hat{r}^3}}, \tag{2}$$

$$\mathscr{C} = 1 - \frac{3}{2\hat{r}} + 2a_*\sqrt{\frac{1}{8\hat{r}^3}}, \tag{3}$$

$$\mathscr{D} = 1 - \frac{1}{\hat{r}} + \frac{a_*^2}{4\hat{r}^2}, \tag{4}$$

$$\mathscr{E} = 1 + \frac{a_*^2}{\hat{r}^2} - \frac{a_*^2}{2\hat{r}^3} + \frac{3a_*^4}{16\hat{r}^4}, \tag{5}$$

$$\mathscr{F} = 1 - 2a_*\sqrt{\frac{1}{8\hat{r}^3}} + \frac{a_*^2}{4\hat{r}^2}, \tag{6}$$

$$\Omega_k = \sqrt{\frac{GM}{R^3}}\frac{1}{\mathscr{B}}, \tag{7}$$

$$l_k = \sqrt{GMR}\frac{\mathscr{F}}{\mathscr{C}^{1/2}}, \tag{8}$$

where $a_* = cJ/GM^2$ is the dimensionless spin parameter of a black hole, $\hat{r}(=R/R_s)$, J, $R_s = 2GM/c^2$, and M are the dimensionless radius, angular momentum of a black hole, Schwarzschild radius, and black hole mass, respectively.

As in PLC21, the general relativistic continuity equation for the outer thin disk with winds driven by a large-scale magnetic field can be written as:

$$\frac{d\dot{M}}{dR} + 4\pi R\dot{m}_w = 0, \tag{9}$$

where $\dot{m}_w$ is the mass-loss rate per unit surface area of the disk (see PLC21 for the details).

The angular momentum equation can be rewritten as

$$-\frac{1}{2\pi}\frac{d(\dot{M}l_k)}{dR} - \frac{d}{dR}(R^2\mathscr{B}\mathscr{C}^{-1/2}\mathscr{D}T_{r\phi}) + T_m R = 0, \tag{10}$$

where $T_{r\phi}$ and T_m are the viscous and the magnetic torques exerted on the accretion disk, respectively (see PLC21 for the details).

While the viscosity in the accretion disk is believed to be related to the turbulence induced by the magnetorotational instability (MRI; Balbus & Hawley 1998), the viscous torque has been suggested to be either proportional to the total pressure (Shakura & Sunyaev 1973), proportional to the gas pressure (Sakimoto & Coroniti 1981), or both (Czerny et al. 2009). In this work, we adopt a general form for the viscous torque:

$$T_{r\phi} = -2\alpha P_{tot}^{1-\mu}P_{gas}^{\mu}H, \tag{11}$$

where P_{tot} and P_{gas} are the total pressure and gas pressure, respectively (Horiuchi & Kato 1990; Done & Davis 2008). This choice is directly motivated by the requirement that the outer radius of unstable zone should be close enough to ISCO with the parameters presented in Section 3, in order to get a narrow unstable zone. The widely used α-viscosity is $\nu = -\alpha C_s H(d\ln\Omega_k/d\ln R)^{-1}$ (and $T_{r\phi} = \nu\Sigma R d\Omega_k/dR$), where C_s is sound speed of the local disk and $H = (P_{tot}/\rho)^{1/2}\Omega_k^{-1}$ is the half thickness of the disk. With $C_s = (P_{tot}/\rho)^{1/2}$, we have $\nu \propto \alpha P_{tot}$ (Shakura & Sunyaev 1973), corresponding to $\mu = 0$ in Equation (11). Taam & Lin (1984) proposed that the turbulent velocity may be related to sound speed $C_s = (P_{gas}/\rho)^{1/2}$ instead of $C_s = (P_{tot}/\rho)^{1/2}$, which leads to $\nu \propto \alpha(P_{gas}P_{tot})^{1/2}$, i.e., $\mu = 0.5$. In this case, the thermal instability of the disk is mostly suppressed. The parameter of μ in this work is employed to describe to what extent the turbulent velocity depends on the gas pressure. The exact value of μ is currently unknown, as is its physical interpretation. Stability criteria applied to X-ray binary systems suggest $\mu \sim 0.56$ (see Done & Davis 2008 for details). However, in this work we are not attempting to model the general behavior of accreting black holes, but rather to seek a possible explanation of a relatively rare phenomenon (QPEs) in terms of disk instabilities. As such, as discussed in Section 3, we adopt a value of $\mu = 0.27$ that allows for a small instability region close to the ISCO without affecting the stability of the outer disk.

The total pressure reads:

$$P_{tot} = \left(1 + \frac{1}{\beta_1}\right)(P_{gas} + P_{rad}), \tag{12}$$

where $\beta_1 = (P_{gas} + P_{rad})/(B^2/8\pi)$; B and P_{rad} are magnetic strength and radiation pressure, respectively. In the standard thin disk model, the zero viscous torque condition is usually adopted at ISCO. However, an additional magnetic torque would be exerted on the ISCO when large-scale magnetic fields are present (e.g., Krolik 1999). The nonzero torque on the inner boundary will increase the radiative efficiency by producing additional dissipation (e.g., Agol & Krolik 2000). Following Agol & Krolik (2000), we define a parameter f in our model to describe the effect of the nonzero torque condition at ISCO in

the Kerr metric:

$$T_{r\phi}\bigg|_{R=R_{\rm ISCO}} = -(1-f)\left[\frac{\dot{M}l_{\rm k}\mathscr{C}^{1/2}}{2\pi\mathscr{B}\mathscr{D}R^2}\right]_{R=R_{\rm ISCO}}, \qquad (13)$$

where the parameter f can be related to the parameter $f_{\rm ms}$ in Agol & Krolik (2000) as:

$$f_{\rm ms} = \frac{3(1-f)}{2x_{\rm ms}^2\mathscr{C}_{\rm ms}^{1/2}}. \qquad (14)$$

Our f parameter can take any value between $-\infty$ and 1, while f_{ms} is limited to vary between 0 and ∞. The zero-torque condition corresponds to $f=1$ in our model instead of $f_{\rm ms}=0$.

Without an inner ADAF region, the energy equation will return to the classical form as:

$$-\frac{3}{2}\Omega_{\rm k}T_{r\phi}\frac{\mathscr{B}\mathscr{D}}{\mathscr{C}} = \frac{8acT_{\rm c}^4}{3\tau}. \qquad (15)$$

The optical depth τ is given by $\tau = \bar{\kappa}\Sigma/2$, where $\bar{\kappa}$ and $\Sigma = 2\rho H$ are the opacity and surface density, respectively.

2.2. Variable Inner Unstable Region

The instability of a standard thin accretion disk in the Kerr metric had been investigated by Xue et al. (2011), where the continuity equation is given as:

$$u^t\frac{\partial\Sigma}{\partial t} = -\frac{1}{r}\frac{\partial}{\partial r}(\Sigma r u^r) - \Sigma\frac{\partial u^t}{\partial t}, \qquad (16)$$

where u^t and u^r are the time and radial components of four-velocity, respectively. Similar to PLC21, the Equation (16) can be rewritten as:

$$\left[u^t - \frac{C_{\rm H}H(1-\beta_2)}{\Sigma(1+\beta_2)}\right]\frac{{\rm d}\Sigma}{{\rm d}t} + \frac{C_{\rm H}H(4-3\beta_2)}{T(1+\beta_2)}\frac{{\rm d}T}{{\rm d}t}$$
$$- \frac{\dot{M}_0 - \dot{M} - 4\pi R\dot{m}_{\rm w}\Delta R}{2\pi R\Delta R} = 0, \qquad (17)$$

where $\dot{M}_0$ and ΔR are the inflow rate and the width of the unstable zone, respectively. $\beta_2 = P_{\rm gas}/(P_{\rm gas} + P_{\rm rad})$ is the ratio of gas pressure to the sum of gas pressure and radiation pressure. In order to simplify the form of the equation, we define a coefficient $C_{\rm H}$ as:

$$C_{\rm H} = -\frac{u^t u^r\Sigma\dot{M}_0}{2\pi RH_0\Sigma_0[c^2\mathscr{D} + (u^r)^2]}, \qquad (18)$$

where H_0 and Σ_0 are the scale-height and surface density on the outer boundary of unstable zone, respectively.

The energy conservation equation is (Xue et al. 2011):

$$\Sigma T\left[u^t\frac{\partial S}{\partial t} + u^r\frac{\partial S}{\partial r}\right] = Q^+ - Q^-, \qquad (19)$$

where S, Q^+, and Q^- are the entropy of gas, the viscous heating rate, and the cooling rate, respectively. The second term on the left side of Equation (19) represents the advection rate of energy $Q_{\rm adv}$, which can be written as (see PLC21):

$$Q_{\rm adv} = \frac{\dot{M}PH}{2\pi R\Delta R\Sigma\mathscr{D}^{\frac{1}{2}}}. \qquad (20)$$

Table 1
Detailed Parameter of Our Fitting

Number	M	a_*	f	$\dot{m}$	α	β_1	μ
1	2×10^5	0.98	0.9	0.08	0.15	38	0.27
2	4×10^5	0.98	0.9	0.08	0.15	22	0.3
3	2×10^5	0.98	1	0.08	0.15	50	0.24
4	2×10^5	0.9	0.9	0.08	0.15	35	0.25

Therefore, the evolution equation of temperature can be rewritten as:

$$\frac{{\rm d}T}{{\rm d}t} = \frac{T\left(Q^+ - Q^- - Q_{\rm adv}\right)\left(1 + \frac{1}{\beta_1}\right)(1+\beta_2)}{2PHu^t\left(28 - 22.5\beta_2 - 1.5\beta_2^2 + \frac{12-9\beta_2}{\beta_1}\right)}$$
$$+ 2\frac{T{\rm d}\Sigma}{\Sigma{\rm d}t}\frac{4 - 3\beta_2 + \frac{2-\beta_2}{\beta_1}}{28 - 22.5\beta_2 - 1.5\beta_2^2 + \frac{12-9\beta_2}{\beta_1}}. \qquad (21)$$

3. Numerical Results

With Equations (17) and (21), we can study the limit-cycle behavior of the thin disk. The overall model is complex and depends on several free parameters. Exploring the full parameter space to compare the model with the available X-ray data would require one to generate a very large number of simulations that would take decades to run. Moreover, the large number of free parameters that is inherent to any disk instability model implies that general model predictions can be obtained, but that different details can be produced easily. This suggests that one should look for qualitative comparisons with the data rather than detailed fits, at least in this initial stage. We adopt here a fiducial model with a black hole mass of $2\times10^5 M_\odot$ and a high black hole spin value of 0.98. A discussion on the choice of parameters for the fiducial model is given in Section 4. This value of mass is 2 times smaller than that given by Miniutti et al. (2019), but is still in range with the estimated black hole mass. Other parameters are conveniently chosen as $f=0.9$, $\dot{m}=0.08\dot{M}_{\rm Edd}$ ($\dot{M}_{\rm Edd} = 1.5\times10^{18}M/M_\odot$ g s^{-1}), $\alpha=0.15$, $\beta_1=38$, $\mu=0.27$, and $\Delta R=0.12R_{\rm s}$ (see Group 1 in Table 1). Here the outer radius of ΔR is given self-consistently by the disk instability criteria (see Section 4 for details).

GSN 069 is observed to display QPEs about every 9 hr. During the outbursts, the X-ray flux can increase by about 2 orders of magnitude (Miniutti et al. 2019). We compare the results of our model with the observed quasi-periodic 0.4–2 keV light curve of GSN 069 in Figure 2. It is found that our theoretical results can qualitatively fit both the period and the outburst duration, although the alternating strong/weak peaks and short/long recurrence times are not well reproduced. Furthermore, in Figure 3, we present the normalized light curves for the three different energy bands given by Figure 2(b) of Miniutti et al. (2019). The narrower width found in high-energy bands is also qualitatively consistent with observational results of GSN 069. On the other hand, QPEs in higher energy bands peak earlier in GSN 069, and our model does not reproduce this behavior.

The timing properties of GSN 069 have been reproduced by several works (e.g., King 2020; Raj & Nixon 2021;
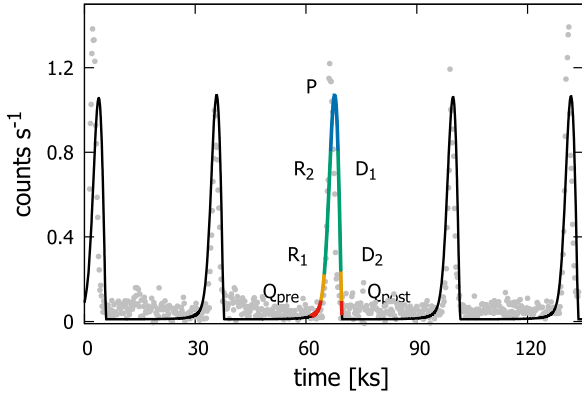
3

Figure 2. The 0.4–2 keV light curve, where the black line represents the light curve given by our model and the colored lines are the seven phase segments of eruption to fit the X-ray spectrum in Figure 4. The gray dots are the data observed by XMM-Newton Director Discretionary Time (DDT) performed on 2019 January 16/17.
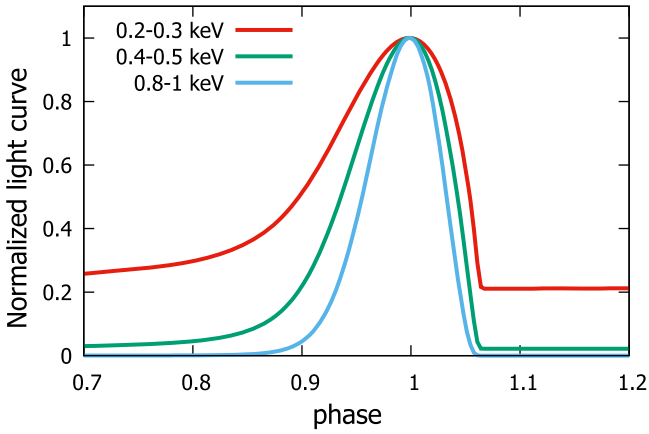

Figure 3. The light curves normalized by the peak flux in three different energy bands. The red, green, and blue lines correspond to the 0.2–0.3 keV, 0.4–0.5 keV, and 0.8–1 keV light curves, respectively.

Xian et al. 2021). However, besides the timing properties, the X-ray spectrum during outburst has also been well resolved by XMM-Newton (see Figure 4 in Miniutti et al. 2019, where a whole outburst is divided into seven phases). We adopt seven phase segments of outburst (Q_{pre}, R_1, R_2, P, D_1, D_2, and Q_{post}, see the colored lines in Figure 2) to fit the observed X-ray spectrum. It is found that all the X-ray spectra during outburst can be qualitatively reproduced by our model. The average effective temperatures of the unstable zones corresponding to the seven segments are $kT_{Q_{pre}} = 57 eV$, $kT_{R_1} = 67 eV$, $kT_{R_2} = 81 eV$, $kT_P = 91 eV$, $kT_{D_1} = 82 eV$, $kT_{D_2} = 68 eV$, and $kT_{Q_{post}} = 59 eV$, respectively. The phase-resolved X-ray data in Figure 4 are taken from Figure 3 in Miniutti et al. (2019) after correcting the instrumental effective area and galaxy absorption, in which the cross-sections given by Morrison & McCammon (1983) and the equivalent hydrogen column n_H ($= 3 \times 10^{20} cm^{-2}$) are adopted. Some of the spectra show a high-energy excess with respect to our model prediction, i.e., the agreement is qualitative but there is still room for improvement, as discussed in the following section.

4. Choice of Parameters in Our Model

In addition to the width of the unstable region ΔR, our model includes seven free parameters, i.e., the black hole mass
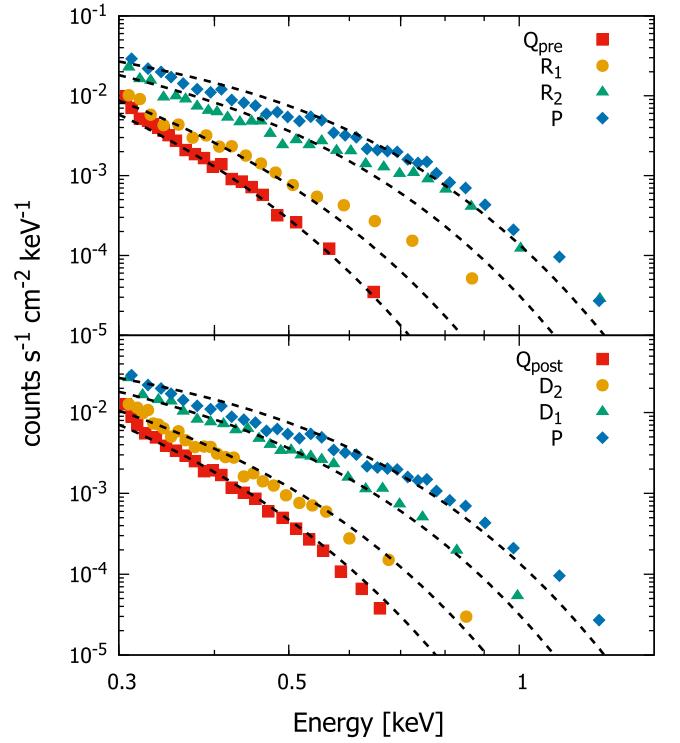

Figure 4. Phase-resolved Spectral analysis of GSN 069. The colored points with various shapes are the observational data after doing corrections of instrumental effective area and absorption.

M, black hole spin a_*, f, mass accretion rate $\dot{m}$, α, β_1, and μ. ΔR is self-consistently given by the disk instability criteria given in Kato et al. (1998), which indicates that the disk is unstable when $4 - 10\beta_2 - 7\mu + 7\beta_2\mu > 0$, where β_2 is determined by the mass accretion rate and radius. There are five main characteristics required to fit the data points in Figures 2 and 4 well, i.e., (1) the eruption period; (2) the eruption duration and shape; (3) the amplitude of eruption; (4) the constant temperature component during spectral evolution (representing the constant outer disk emission); and (5) a variable temperature component during spectral evolution. As mentioned, our goal here is to provide a possible framework for QPE production, obtaining results that are close enough, both in timing and spectral properties, to the observed data to suggest that this type of modeling is worth exploring further in the future.

The maximal disk temperature inferred from observation is $kT_{max} \sim 50 eV$. However, for a thin accretion disk surrounding a black hole with mass of $4 \times 10^5 M_\odot$, the maximal disk temperature is only $kT_{max} \sim 30 eV$ ($kT_{max} = 11.5(M/10^8 M_\odot)^{-1/4} \dot{m}^{1/4}$ (eV)). In order to match the disk temperature before outburst (the constant temperature component), a small black hole mass $2 \times 10^5 M_\odot$, a high black hole spin ($a = 0.98$), and a nonzero viscous torque are all simultaneously necessary at the first step. We notice that a spectral hardening factor κ (~ 1.7) between the effective temperature of the disk T_{eff} and the observed disk temperature T_{max} ($T_{max} \sim \kappa T_{eff}$) is adopted in Miniutti et al. (2019) when fitting the black hole mass. With the parameter κ, a disk temperature $T_{eff} \sim 30 eV$ is enough to fit the observed spectra. In this case, a black hole with mass of $4 \times 10^5 M_\odot$ should be able to fit the observational data well. Our model ignores any spectral hardening, and therefore the matching with the observed constant temperature can only be obtained with a smaller black hole mass.
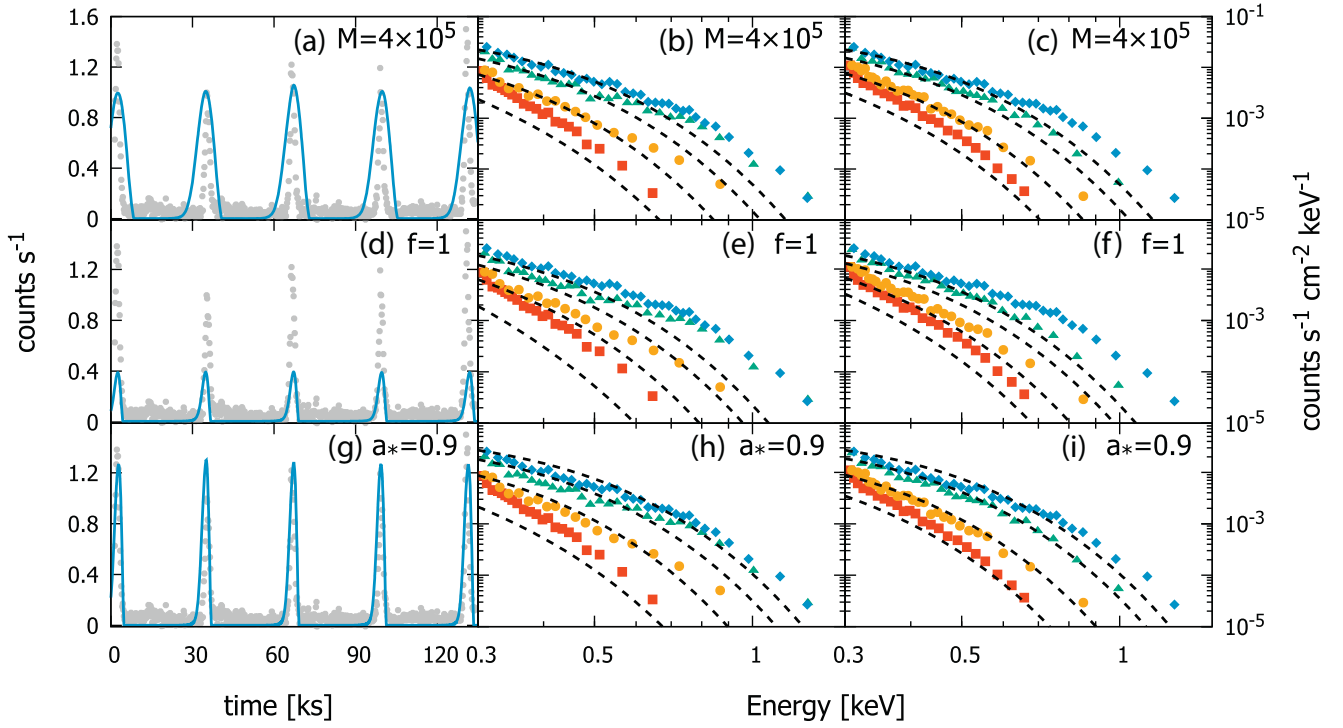
Figure 5. The 0.4–2 keV light curves and phase-resolved spectral analysis under different parameter groups. Panels (a)–(c), (d)–(f), and (g)–(i) correspond to $M = 4 \times 10^5 M_\odot$, $f = 1$ (zero-torque condition), and $a_* = 0.9$, respectively. The best-fitting parameters of panels (a)–(c), (d)–(f), and (g)–(i) correspond to Group 2, Group 3, and Group 4 in Table 1, respectively.

In Figure 5(a)–(c), we investigate the effects of black hole mass M on the 0.4–2 kev light curves and phase-resolved spectral analysis. During the process of fitting, the eruption period and duration are the first two characteristics that should be matched. It is found that the parameters with $M = 4 \times 10^5 M_\odot$ (the detailed parameters adopted are listed in Table 1) can reproduce a similar evolution trend for both the light curves and the spectral analysis, but provide a much worse match to the data. The worse fit of the spectral evolution (see Figure 5(b) and (c)) is driven by a too low constant temperature of the thermal component that is present in all fits, and could likely be cured by introducing a hardening factor, as explained above. On the other hand, QPEs have the right recurrence time but are too long (broad), as shown in Figure 5(a). However, if the mismatch of the spectral evolution fits can be ignored due to the hardening factor, the QPEs may be made narrower (shorter) by playing with a small value of μ (see Figure 6). Next, we adjust the other four parameters (α, β_1, μ, and $\dot{m}$) to reproduce the other four characteristics observed. The parameters μ can change the ratio of eruption duration to the period (see Figure 6). How the last three parameters affect the outburst behavior has been reported by PLC21. It is found that the stronger magnetic field strength (smaller β_1) will result in both a decreasing eruption period and higher eruption amplitude. However, increasing α can only increase the eruption period (see PLC21 for details). The increase of mass accretion rate will improve the maximal disk temperature ($T_{max} \sim \dot{m}^{1/4}$) and the width of the unstable zone, resulting in the enhancement of all five characteristics.

The nonzero torque in Equation (13) will emerge when considering the magnetic torque exerted on the gas at ISCO by the in-falling gas inside the ISCO (Krolik 1999). However, this torque should be small due to the small scale-height and the weak magnetic field in a thin disk (Nixon & Pringle 2021), which is also suggested by GRMHD simulations (Noble et al. 2010). In our model, a small nonzero torque $f = 0.9$ (~10% of the angular

momentum at ISCO) is adopted, which is consistent with the results of simulations ($f = 1$ corresponding to the zero-torque condition). We give the results with zero torque in Figure 5(d)–(f). It is found that the results with nonzero torque are much better than that with zero torque because the effective gas temperature close to ISCO can be greatly increased with nonzero torque (the effective temperature at ISCO is zero for zero torque).

The spin of black hole is adopted as 0.98 in this work. As discussed by Thorne (1974), the maximal black hole spin can reach 0.998. However, the maximal value of spin will be smaller than 0.998 when taking the nonzero torque into account, which seems to be inconsistent with our assumption. However, the torque at ISCO is small as suggested by the MHD simulations and thus it will not affect the maximal value of spin significantly. Furthermore, QPEs are likely transient phenomena in the accretion history of a given source (no QPEs are observed in GSN 069 after June 2020), and if they correspond to nonzero torque transient phases, the black hole spin could well have been established during past long-lived zero-torque phases (Shu et al. 2018). Our model only allows a slightly lower BH spin in order to fit the observational data well (see Figure 5(g)–(i)), the fitting results with $a_* = 0.9$ are a little worse but still acceptable). Finally, although the width of the unstable region is small ($\Delta R = 0.12 R_s$), it can still significantly change the 0.4–2 kev light curve (Figure 2). However, the variation of bolometric luminosity is less than 20% for the reason that the light curves are almost constant at optical-UV bands, which is consistent with observational results (Miniutti et al. 2019).

5. Conclusions and Discussion

The mechanism of QPEs is still unclear. In this work, we adopt a disk instability model to explore the physical origin of QPEs in GSN 069. The model of PLC21 is improved by (1)
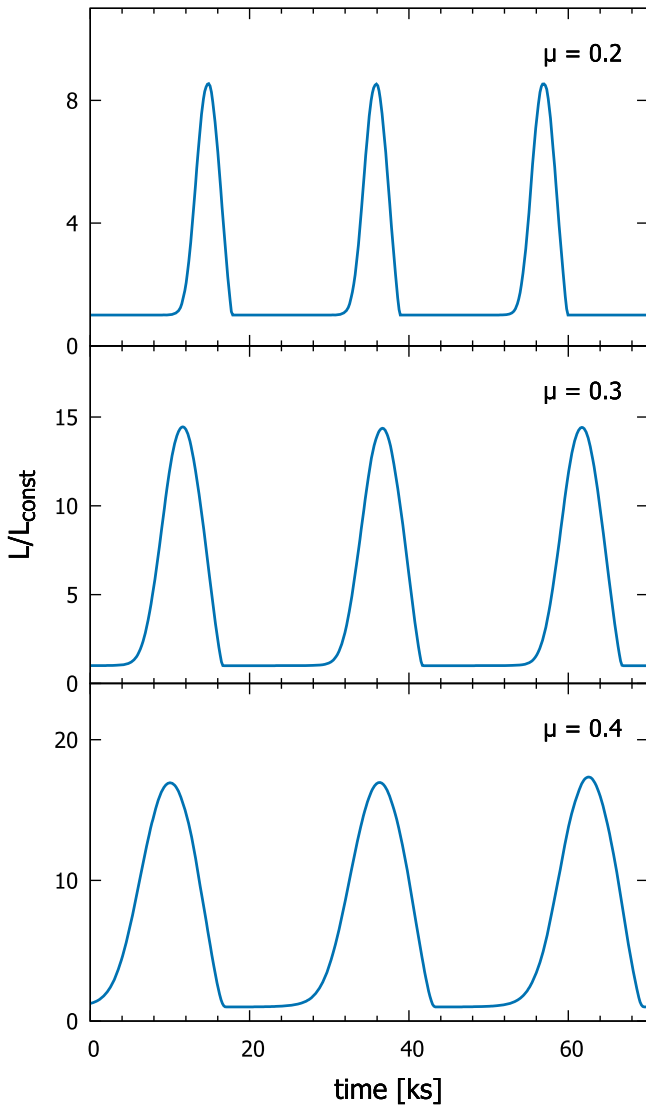
Figure 6. The 0.4–2 keV light curve, where $L_{\rm const}$ is the luminosity of outer constant disk and the value of μ in the top, middle, and bottom panels are 0.2, 0.3, and 0.4, respectively. Other parameters adopted in this figure are $f = 0.9$, $\dot{m} = 0.1 M_{\rm Edd}$, $\alpha = 0.15$, $\beta_1 = 50$, and $\Delta R = 0.1 R_{\rm s}$.

importing the nonzero torque on the inner boundary of thin disk, (2) adopting a general form of viscous stress tensor ($T_{r\phi} = -2\alpha P_{\rm tot}^{1-\mu} P_{\rm gas}^{\mu} H$), and (3) adopting the Kerr metric. Our model can qualitatively fit the 0.4–2 keV light curves, the light curves at different energy bands, and the phase-resolved X-ray spectrum (Figures 2, 3 and 4). However, we emphasize that the parameters adopted above may not represent the real best-fitting set. Exploring the full parameter space is, however, beyond the scope of this work as a full set of simulations would require several decades of computing time (by personal computer). A more quantitative comparison with data could be possible by fixing some/several free parameters to fiducial values, and by considering only a limited set of variable ones. We defer this study to future work.

The period, outburst duration, and light-curve profile of QPEs are source-dependent (see, e.g., Miniutti et al. 2019; Giustini et al. 2020; Arcodia et al. 2021). The period and amplitude of an outburst can be changed significantly by the presence of large-scale magnetic field (PLC21). Furthermore, we suggest that the μ parameter in the general form of viscous

torque can be a useful tool to fit the light-curve profile of QPEs (Figure 6). It is found that the ratio of outburst duration to the period increases with increasing μ, which means that our model may also be applicable to other QPEs. Although our model can qualitatively fit the characteristics of light curves in GSN 069, some observational details are still problematic for our toy model, e.g., the asymmetric eruptions (a faster rise and slower decay is seen in some of the QPE sources); the peak delay at different energy bands (the flux of higher energy bands peak at earlier times); the hard X-ray excess ($\sim$1keV) that is not well reproduced by our model during the R_1, R_2, and P phases; and the alternating long/short and strong/weak QPEs. The first two issues may be resolved if we allow the unstable zone to propagate outwards instead of remaining constant (Li et al. 2007), the radiative area of the unstable zone will increase after eruption and result in asymmetric eruptions and peak delay at different energy bands. The hard X-ray excess at R_1, R_2, and P phases may be related to the appearance of a warm Comptonizing corona, as generally observed in AGN (Petrucci et al. 2020). The alternating strong/weak QPEs and long/short recurrence times may be partly solved if the unstable zone is variable instead of a constant due to the slight variation of magnetic field, perhaps responding to the QPEs themselves in a sort of feedback loop. We can expect a longer recurring time when the eruptions are stronger, which will drag more gas from the accretion disk into the black hole. We will further investigate these issues in future work.

ORCID iDs

Xin Pan ⓘ https://orcid.org/0000-0002-6938-3594
Shuang-Liang Li ⓘ https://orcid.org/0000-0002-7299-4513
Xinwu Cao ⓘ https://orcid.org/0000-0002-2355-3498
Giovanni Miniutti ⓘ https://orcid.org/0000-0003-0707-4531
Minfeng Gu ⓘ https://orcid.org/0000-0002-4455-6946

References

Agol, E., & Krolik, J. H. 2000, ApJ, 528, 161
Arcodia, R., Merloni, A., Nandra, K., et al. 2021, Natur, 592, 704
Balbus, S. A., & Hawley, J. F. 1998, RvMP, 70, 1
Cao, X., & Spruit, H. C. 2013, ApJ, 765, 149
Chakraborty, J., Kara, E., Masterson, M., et al. 2021, ApJL, 921, L40
Czerny, B., Siemiginowska, A., Janiuk, A., Nikiel-Wroczyński, B., & Stawarz, Ł. 2009, ApJ, 698, 840
Done, C., & Davis, S. W. 2008, ApJ, 683, 389
Giustini, M., Miniutti, G., & Saxton, R. D. 2020, A&A, 636, L2
Horiuchi, T., & Kato, S. 1990, PASJ, 42, 661
Ingram, A., Motta, S. E., Aigrain, S., & Karastergiou, A. 2021, MNRAS, 503, 1703
Kato, S., Fukue, J., & Mineshige, S. 1998, in Black-hole Accretion Disks, ed. S. Kato, J. Fukue, & S. Mineshige (Kyoto Univ. Press: Kyoto)
King, A. 2020, MNRAS, 493, L120
Krolik, J. H. 1999, ApJL, 515, L73
Li, J., & Cao, X. 2019, ApJ, 872, 149

Li, S.-L., & Begelman, M. C. 2014, ApJ, 786, 6
Li, S.-L., Xue, L., & Lu, J.-F. 2007, ApJ, 666, 368
Metzger, B. D., Stone, N. C., & Gilbaum, S. 2022, ApJ, 926, 101
Miniutti, G., Saxton, R. D., Giustini, M., et al. 2019, Natur, 573, 381
Morrison, R., & McCammon, D. 1983, ApJ, 270, 119
Narayan, R., Mahadevan, R., & Quataert, E. 1998, in Theory of Black Hole
    Accretion Disks, ed. M. A. Abramowicz, G. Björnsson, & J. E. Pringle
    (Cambridge: Cambridge Univ. Press)
Nixon, C. J., & Pringle, J. E. 2021, NewA, 85, 101493
Noble, S. C., Krolik, J. H., & Hawley, J. F. 2010, ApJ, 711, 959
Novikov, I. D., & Thorne, K. S. 1973, in Black Holes (Les Astres Occlus), ed.
    C. DeWitt & B. DeWitt (London: Gordon and Breach), 343
Pan, X., Li, S.-L., & Cao, X. 2021, ApJ, 910, 97
Petrucci, P. O., Gronkiewicz, D., Rozanska, A., et al. 2020, A&A, 634, A85

Raj, A., & Nixon, C. J. 2021, ApJ, 909, 82
Sakimoto, P. J., & Coroniti, F. V. 1981, ApJ, 247, 19
Shakura, N. I., & Sunyaev, R. A. 1973, A&A, 24, 337
Shakura, N. I., & Sunyaev, R. A. 1976, MNRAS, 175, 613
Sniegowska, M., Czerny, B., Bon, E., & Bon, N. 2020, A&A, 641, A167
Suková, P., Zajaček, M., Witzany, V., & Karas, V. 2021, ApJ, 917, 43
Sun, L., Shu, X., & Wang, T. 2013, ApJ, 768, 167
Taam, R. E., & Lin, D. N. C. 1984, ApJ, 287, 761
Thorne, K. S. 1974, ApJ, 191, 507
Xian, J., Zhang, F., Dou, L., He, J., & Shu, X. 2021, ApJL, 921, L32
Xue, L., Sądowski, A., Abramowicz, M. A., & Lu, J.-F. 2011, ApJS, 195, 7
Zhao, Z. Y., Wang, Y. Y., Zou, Y. C., Wang, F. Y., & Dai, Z. G. 2021,
    arXiv:2109.03471
Shu, X. W., Wang, S. S., Dou, L. M., et al. 2018, ApJL, 857, L16